

Constraining Anomaly Mediated Supersymmetry Breaking Framework via Ongoing Muon $g - 2$ Experiment at Brookhaven

Utpal Chattopadhyay^{a1}, Dilip Kumar Ghosh^{b2}, and Sourov Roy^a

*^aDepartment of Theoretical Physics
Tata Institute of Fundamental Research
Homi Bhabha Road, Mumbai 400 005, India*

^bCERN, Theory Division, CH-1211 Geneva 23, Switzerland

Abstract

The ongoing high precision E821 Brookhaven National Laboratory experiment on muon $g - 2$ is promising to probe a theory involving supersymmetry. We have studied the constraints on minimal Anomaly Mediated Supersymmetry Breaking (AMSB) model using the current data of muon $g - 2$ from Brookhaven. A scenario of seeing no deviation from the Standard Model is also considered, within 2σ limit of the combined error from the Standard Model result and the Brookhaven predicted uncertainty level. The resulting constraint is found to be complementary to what one obtains from $b \rightarrow s + \gamma$ bounds within the AMSB scenario, since only a definite sign of μ is effectively probed via $b \rightarrow s + \gamma$. A few relevant generic features of the model are also described for disallowed regions of the parameter space.

PACS numbers: 12.60.Jv, 04.65.+e, 13.40.Em, 14.60.Ef

¹utpal@theory.tifr.res.in, Dilip.Ghosh@cern.ch, sourov@theory.tifr.res.in

²On leave of absence from Department of Theoretical Physics, TIFR, Mumbai, India.

1 Introduction

Search for supersymmetry (SUSY) in high energy physics relies both on the high energy colliders, as well as on the experiments based on perturbative corrections to various experimentally measurable quantities. Traditionally, measurement of electron's anomalous magnetic moment has been highly effective to verify the prediction of quantum electrodynamics (QED) to a very high order. Probing a Beyond the Standard Model physics with supersymmetry has been seen to be possible with a precision $(g - 2)$ measurement of muon. The ongoing muon $(g - 2)$ measurement E821[1] at Brookhaven National Laboratory (BNL), designed to verify the results of Standard Model (SM) electroweak corrections, has already provided more accurate result than the previous CERN experiment[2], by a factor of 2 or so. With improved design and state of the art technology, it is expected that within a few years from now, the accuracy of the BNL result will be increased by a factor of 20, or even more, compared to the same of the previous CERN measurement.

Supersymmetric electroweak corrections to muon $(g - 2)$ can be as large as the SM electroweak correction, and this fact has been seen in a number of references ranging from the minimal supersymmetric standard model (MSSM)[3, 4], Supergravity based models[5, 6], and Gauge Mediated Supersymmetry Breaking scenarios[7]. In the recent past, considerable interest has been seen in a different type of SUSY breaking mechanism, other than Supergravity [8] and Gauge Mediated SUSY Breaking[9], which at its dominating scenario, is generically known as Anomaly Mediated Supersymmetry Breaking (AMSB) [10–12]. This effect originates from the existence of Super-Weyl anomaly[10] while considering SUSY breaking. As we will discuss latter, the resulting tachyonic sleptons within AMSB sparticle spectrum is avoided in the *minimal* definition[13–18] of the model, by adding a common scalar mass m_0 with all the scalars of the theory at a given scale.

Large SUSY contributions $a_\mu^{\text{SUSY}} \equiv \frac{1}{2}(g - 2)_\mu^{\text{SUSY}}$ in the minimal AMSB framework has already been seen in Ref. [13], in which the authors discussed in detail, a broad range of interesting phenomenological implications involving colliders, as well as various low energy signatures within the same model, besides showing that the minimal model may remain *natural* even for a super-heavy m_0 . In this work, we will analyze the constraint coming from a_μ^{SUSY} in regard to the high-precision Brookhaven experiment, within minimal AMSB framework. Considering $a_\mu^{\text{exp}} - a_\mu^{\text{SM}} = a_\mu^{\text{SUSY}}$, while taking into account the associated error

limits in quadratures, we will constrain the SUSY parameter space of the AMSB model under discussion.

Our work will be organized as follows. In Section 2, we will discuss the SM result for a_μ for its different parts of contributions. We will see the existence of a large error associated with the lowest order hadronic vacuum polarization contribution, and sources of its possible improvement in the near future, via low energy $e^+e^- \rightarrow hadrons$ data from various experiments. We will describe the AMSB framework, and the necessity of defining a *minimal* scenario in Section 3. In Section 4, we will use Ref. [5] for the result of a_μ^{SUSY} , where the analysis was performed in the minimal supergravity (mSUGRA) model to see the constraint from the high precision BNL experiment. We will analyze the constraint from a_μ^{SUSY} on the parameter space of the minimal AMSB model, due to the present SM and experimental results of a_μ . We will also investigate the potential for constraining the minimal AMSB model using the predicted level of uncertainty of E821 BNL experiment. We will do so in the minimal *no-deviation* scenario, which here means seeing no disagreement from SM result within the experimental and the theoretical uncertainties, once the measurement is complete at the desired level of accuracy. We will also quote the result of $b \rightarrow s + \gamma$ constraint for both signs of μ , and the positive role of a_μ^{SUSY} analysis in this regard. In Section 5, we will comment on the disallowed regions which appear due to reasons other than a_μ^{SUSY} limits. Primarily, we will examine the disallowed regions of parameters space due to the combined effect of the scale invariant part of the scalar mass relations of sleptons with gauge and Yukawa couplings within the minimal AMSB model, and the nature of the associated renormalization group evolutions. We will also see the effect of SUSY-QCD corrections to the bottom-quark mass on the minimal AMSB spectra, a large $\tan\beta$ effect, which also has specific features within AMSB models. These regions, when combined with a_μ^{SUSY} -eliminated parameter space, provide simpler and definite predictions for the lower bounds of masses of relevant supersymmetric particles, as well as on the input parameters of the model.

2 Standard Model result a_μ^{SM} and sources of uncertainty

The Standard Model result for a_μ is:

$$\frac{1}{2}(g-2)_\mu^{\text{SM}} = a_\mu^{\text{SM}} = 11659162.8(6.5) \times 10^{-10} \equiv (11659162.8 \pm 6.5) \times 10^{-10} \quad (1)$$

In contrast, the latest data from the ongoing E821 BNL experiment[1] amounts to:

$$a_\mu^{\text{exp}} = 11659210(46) \times 10^{-10} \quad (2)$$

The uncertainty amount is expected to be reduced to $\delta a_\mu^{\text{BNL}} \lesssim 4 \times 10^{-10}$.

Table 1: Contributions to a_μ^{SM} (in units of 10^{-10})

Nature of Contribution	Value
Q.E.D. to $O(\alpha/\pi)^5$ [19] (a_μ^{QED})	11658470.6(0.3)
Hadronic vac. polarization to $O(\alpha/\pi)^2$ (a_μ^{had1})[20]	692.4(6.2)
Hadronic vac. polarization to $O(\alpha/\pi)^3$ [21]	-10.1(0.6)
Light by light hadronic amplitude[22]	-5.2(1.8)
Total hadronic (a_μ^{Hadronic})	677.1(6.5)
Total electro-weak up to 2-loops (a_μ^{EW})	15.1(0.4)
a_μ^{SM}	11659162.8(6.5)

The SM result is broken up into:

$$a_\mu^{\text{SM}} = a_\mu^{\text{QED}} + a_\mu^{\text{Hadronic}} + a_\mu^{\text{EW}} \quad (3)$$

Here a_μ^{QED} is the pure QED contribution computed up to five loops in electromagnetic coupling. a_μ^{Hadronic} refers to the total hadronic contribution including the lowest order and the next to lowest order hadronic vacuum polarizations, and the light-by-light hadronic contribution. The electroweak part a_μ^{EW} is the SM electroweak contribution up to two loops. The amounts from the individual parts with corresponding references, are summarized in Table (1).

Within a_μ^{Hadronic} , the contribution a_μ^{had1} arising from the α^2 level of hadronic vacuum polarization diagram is the least accurate quantity; and its uncertainty is almost the same as the overall error of a_μ^{SM} . Hence an accurate determination of a_μ^{had1} will be increasingly important for compatibility with the high-precision measurement at BNL, which has an expected level of uncertainty of $\delta a_\mu^{\text{BNL}} \lesssim 4 \times 10^{-10}$. However, the present uncertainty in a_μ^{SM} is quite small compared to the experimental uncertainty level, a situation which is going to be changed within a few years. The largest hadronic contribution a_μ^{had1} is obtained from the total Born cross section (lowest order in QED) for hadron productions in e^+e^- annihilation, a result found via dispersion theory and optical theorem[23]. Accurate low energy $e^+e^- \rightarrow \text{hadrons}$ data hence becomes necessary to lower the uncertainty level. Measurements of low energy hadron production cross sections in BES, CMD-II and DAΦNE[24], will significantly improve the result of a_μ^{SM} . In the recent past, the authors of Ref. [20] used ALEPH data from hadronic τ decay, and QCD sum-rule techniques to evaluate a_μ^{had1} and this improved the hadronic error estimate very significantly. Our analysis uses this result. Further prospects for improving the result of a_μ^{had1} , as well as a critical evaluation of the above estimate may be seen in Ref. [25].

3 Anomaly Mediated Supersymmetry Breaking in the Minimal Scenario

In a supersymmetric theory, additionally, soft SUSY breaking parameters are also contributed via Super-Weyl anomaly, which is a generic feature if SUSY is broken in a supergravity framework. In anomaly mediated supersymmetry breaking scenario, the Super-Weyl anomaly contributions dominate, because the SUSY breaking sector and the visible sector reside in different parallel 3-branes[10] in a string theoretical perspective, and there are no tree-level couplings between the two branes. The form of soft parameters thus generated, are renormalization group (RG) invariant, and at any desired scale, the soft parameters are determined by the appropriate gauge and Yukawa couplings for the same scale. This is particularly interesting to avoid a SUSY flavor problem, because the scale invariance of soft parameters which is provided by special RG trajectories, eliminates the effect of any flavor violating unknown physics possibly existing at a higher scale,

In spite of many desirable features of anomaly mediation, within the framework of minimal supersymmetric standard model (MSSM), one finds that sleptons become tachyonic. In the *minimal* AMSB model such tachyonic sleptons are avoided by introducing an additional common mass parameter m_0 for all the scalars of the theory. But, this obviously violates the scale invariance of the model, whereas preserving the same would be desirable in regard to the flavor changing neutral current (FCNC) constraint. Tachyonic sleptons are avoided differently in non-minimal AMSB models[26], which have appropriate scale invariant scalar mass combinations within RG evolutions; but these are outside the scope of our present work. However, via the existence of focus point [27] of the renormalization group equation (RGE) of $m_{H_u}^2$, for the Higgs scalar mass term, the minimal model allows the possibility of multi-TeV squarks and sleptons without increasing a fine-tuning measure[13], and this is an important feature to address many phenomenological issues.

Scalar masses are hence determined via renormalization group equations of MSSM starting from their respective values at the unification scale ($M_G \sim 1.5$ to 2.0×10^{16} GeV) and leading up to the electroweak scale M_Z , the scale for mass of Z-boson. However, for the first two generations of scalars, because of the negligible first two generation Yukawa couplings, the effect translates to having simply an overall additive constant m_0 at M_G , which would have minimal changes due to RG evolutions.

In this analysis, the evolutions of scalar masses, gauge and Yukawa couplings are computed at two loop level of RGE[28], and trilinear couplings are evolved via one-loop level of the same. Unification of gauge couplings is incorporated with having $\alpha_3(M_Z) \sim 0.118$. For the Higgsino mixing, μ^2 is computed radiatively via electroweak symmetry breaking condition at the complete one loop level of the effective potential[29], while optimally choosing a renormalization scale $Q = \sqrt{(m_{\tilde{t}_1} m_{\tilde{t}_2})}$, the average stop mass scale, for minimization. The analysis also includes supersymmetric QCD correction to bottom quark mass[30], which is considerable for large $\tan\beta$ regions with also having its important features in AMSB scenarios.

With a high degree of predictivity the model is described by the following parameters: the gravitino mass $m_{3/2}$, the common scalar mass parameter m_0 , the ratio of Higgs vacuum expectation values $\tan\beta$, and $sgn(\mu)$. Following Ref. [31], with having the same sign conventions for μ and A -parameters in this work, we see that the masses are given via the couplings as follows.

Gauginos:

$$\tilde{m}_1 = \frac{33}{5} \frac{g_1^2}{16\pi^2} m_{3/2}, \quad \tilde{m}_2 = \frac{g_2^2}{16\pi^2} m_{3/2}, \quad \text{and} \quad \tilde{m}_3 = -3 \frac{g_3^2}{16\pi^2} m_{3/2} \quad (4)$$

Higgs and Third generation scalars:

$$\tilde{m}_i^2 = C_i \frac{m_{3/2}^2}{(16\pi^2)^2} + m_0^2 \quad (5)$$

where, $i \equiv (Q, U, D, L, E, H_u, H_d)$, with C_i 's being given as:

$$\begin{aligned} C_Q &= -\frac{11}{50}g_1^4 - \frac{3}{2}g_2^4 + 8g_3^4 + h_t\hat{\beta}_{h_t} + h_b\hat{\beta}_{h_b}, \quad C_U = -\frac{88}{25}g_1^4 + 8g_3^4 + 2h_t\hat{\beta}_{h_t} \\ C_D &= -\frac{22}{25}g_1^4 + 8g_3^4 + 2h_b\hat{\beta}_{h_b}, \quad C_L = -\frac{99}{50}g_1^4 - \frac{3}{2}g_2^4 + h_\tau\hat{\beta}_{h_\tau}, \quad C_E = -\frac{198}{25}g_1^4 + 2h_\tau\hat{\beta}_{h_\tau} \\ C_{H_u} &= -\frac{99}{50}g_1^4 - \frac{3}{2}g_2^4 + 3h_t\hat{\beta}_{h_t}, \quad \text{and} \quad C_{H_d} = -\frac{99}{50}g_1^4 - \frac{3}{2}g_2^4 + 3h_b\hat{\beta}_{h_b} + h_\tau\hat{\beta}_{h_\tau} \end{aligned}$$

Here, Q and L are the superpartners of quark and lepton doublet fields respectively. The superpartners for singlet quark fields for up and down type are U and D, and the same for singlet lepton is E.

Trilinear couplings:

$$A_t = \frac{\hat{\beta}_{h_t}}{h_t} \frac{m_{3/2}}{16\pi^2}, \quad A_b = \frac{\hat{\beta}_{h_b}}{h_b} \frac{m_{3/2}}{16\pi^2}, \quad \text{and} \quad A_\tau = \frac{\hat{\beta}_{h_\tau}}{h_\tau} \frac{m_{3/2}}{16\pi^2} \quad (6)$$

where $\hat{\beta}$'s are defined by:

$$\begin{aligned} \hat{\beta}_{h_t} &= h_t \left(-\frac{13}{15}g_1^2 - 3g_2^2 - \frac{16}{3}g_3^2 + 6h_t^2 + h_b^2 \right), \quad \hat{\beta}_{h_b} = h_b \left(-\frac{7}{15}g_1^2 - 3g_2^2 - \frac{16}{3}g_3^2 + h_t^2 + 6h_b^2 + h_\tau^2 \right), \\ \text{and} \quad \hat{\beta}_{h_\tau} &= h_\tau \left(-\frac{9}{5}g_1^2 - 3g_2^2 + 3h_b^2 + 4h_\tau^2 \right) \end{aligned}$$

The quantities for the first two generations can be obtained similarly, by considering appropriate Yukawa couplings, which however are neglected in our analysis. We note that, Eq. (4), and Eq. (6) are scale invariant. Hence, having no intrinsic RG evolutions of their own, the masses and the trilinear couplings, may be computed at any scale once the appropriate gauge and Yukawa couplings are known. However, due to the addition of m_0^2 term, which rescues sleptons from being tachyonic, Eq. (5) is not scale invariant. Here the scale for obtaining the mass values of Eq. (5) is chosen as M_G . Thereafter, RG

evolutions of soft scalar parameters and use of electroweak radiative breaking condition at the complete one loop level produce the sparticle mass spectra. One of the important features of minimal AMSB model is that the resulting $SU(2)$ gaugino mass \tilde{m}_2 is quite smaller than \tilde{m}_1 as well as $|\mu|$. Here, we have also incorporated the non-negligible next to leading order (NLO) corrections[14] for gaugino masses. As a result, lighter chargino $\tilde{\chi}_1^\pm$ and lightest neutralino $\tilde{\chi}_1^0$ are wino dominated, indeed they are almost degenerate, with the latter becoming the lightest supersymmetric particle (LSP). This has interesting phenomenological aspects, like what is seen most recently in Ref. [17], where a definite signal in a linear e^+e^- collider could be predicted as a possible minimal AMSB signature. Compared to other SUSY scenarios where the lightest neutralino has a distinctly smaller mass, here this similar mass values of $m_{\tilde{\chi}_1^\pm}$ and $m_{\tilde{\chi}_1^0}$ effectively decreases $|a_\mu^{\text{SUSY}}|$, although a weakly contributing effect. Another striking result of minimal AMSB model is the strong mass degeneracy between left and right sleptons. Consequently, the third and the second generation L-R mixing angles become significantly larger, going up to the maximal limit for a large $\tan\beta$. We will see the strong effect of large smuon L-R mixing on the neutralino loop contributions of a_μ^{SUSY} in Section 4.

4 Results

The diagrams to compute the supersymmetric contributions to muon ($g-2$) as shown in Figs. (1a) and (1b), are divided into chargino-sneutrino loop, and the neutralino-smuon loop. We only quote the chargino part of the result here, which dominates in a_μ^{SUSY} . The neutralino contribution may be seen in Refs. [3, 5]¹. Separating the chargino contributions into chirality diagonal and non-diagonal parts we have,

$$a_\mu^{\text{SUSY}\chi^\pm} = a_\mu^{\text{SUSY}\chi^\pm}(\text{non - diag}) + a_\mu^{\text{SUSY}\chi^\pm}(\text{diag}) \quad (7)$$

where

$$a_\mu^{\text{SUSY}\chi^\pm}(\text{non - diag}) = \frac{m_\mu^2 \alpha_{em}}{4\sqrt{2}\pi m_W \sin^2 \theta_W \cos \beta} \sum_{i=1}^2 \frac{1}{m_{\chi_i^\pm}} (U_{i2} V_{i1}) F\left(\frac{m_{\tilde{\nu}_\mu}^2}{m_{\chi_i^\pm}^2}\right) \quad (8)$$

¹The most general result of SUSY electroweak contribution to muon ($g-2$) in MSSM, where CP violating phases are considered, can be seen in Ref. [3].

and

$$a_\mu^{\text{SUSY}\chi^\pm}(\text{diag}) = \frac{m_\mu^2 \alpha_{em}}{24\pi \sin^2 \theta_W} \sum_{i=1}^2 \frac{1}{m_{\chi_i^\pm}^2} \left(\frac{m_\mu^2}{2m_W^2 \cos^2 \beta} U_{i2}^2 + V_{i1}^2 \right) G \left(\frac{m_{\tilde{\nu}_\mu}^2}{m_{\chi_i^\pm}^2} \right). \quad (9)$$

Here, in general, U and V are unitary 2×2 matrices, which diagonalize the chargino matrix $M_{\tilde{\chi}^\pm}$ as shown below, via bi-unitary transformation, $U^* M_{\tilde{\chi}^\pm} V^{-1} = \text{diag}(m_{\tilde{\chi}_1^\pm}, m_{\tilde{\chi}_2^\pm})$.

$$M_{\tilde{\chi}^\pm} = \begin{pmatrix} \tilde{m}_2 & \sqrt{2} m_W \sin \beta \\ \sqrt{2} m_W \cos \beta & \mu \end{pmatrix} \quad (10)$$

With the chargino matrix being real, the elements of U and V as appearing in Eq. (8-9) correspond to orthogonal matrices. The functions $F(x)$ and $G(x)$ arising from loop-integrations are given by: $F(x) = (3x^2 - 4x + 1 - 2x^2 \ln x)/(x - 1)^3$, and $G(x) = (2x^3 + 3x^2 - 6x + 1 - 6x^2 \ln x)/(x - 1)^4$.

Using the complete a_μ^{SUSY} result for numerical computation, Figs. (2a) and (2b) show the dominance of chargino contributions over the neutralino parts. Here, the two types of contributions are plotted along the axes for $\tan\beta=25$, when $m_{3/2}$ and m_0 are varied over a broad range of values ($m_{3/2} < 100$ TeV and $m_0 < 1$ TeV). It is indeed the chirality non-diagonal term involving the *lighter*-chargino and sneutrino part, which dominates over the other contributions in a_μ^{SUSY} and due to the same reason, as explained further in a similar mSUGRA analysis of Ref. [5], there is a definite sign dependence between a_μ^{SUSY} and μ , namely $a_\mu^{\text{SUSY}} > 0$ for $\mu > 0$, and $a_\mu^{\text{SUSY}} < 0$ for $\mu < 0$, an important result for a_μ^{SUSY} . Thus, the lighter chargino mass ($m_{\tilde{\chi}_1^\pm}$) has a significant role in a_μ^{SUSY} . On the other hand, for a given $m_{\tilde{\chi}_1^\pm}$ value, a heavier $m_{\tilde{\nu}_\mu}$ decreases $|a_\mu^{\text{SUSY}}|$. Due to the presence of Yukawa coupling ($\sim \frac{1}{\cos\beta}$) within the chirality non-diagonal terms for both chargino (see Eq. 8), and neutralino results, we see that $|a_\mu^{\text{SUSY}}|$ is almost proportional to $\tan\beta$.

The special signature of AMSB due to extremely large smuon L-R mixing angle as mentioned before, affects the neutralino results to diminish strongly via partial cancellation between the terms. The particular neutralino term (see Ref. [5]) which involves smuon mixing, becomes almost comparable to the significantly contributing chirality non-diagonal neutralino term associated with Yukawa coupling. Both the terms depend on $\tan\beta$, as well as, on the sign of μ . A detail numerical investigation shows that, the two terms always come opposite in signs, giving a large cancellation within the neutralino result. On a relative scale, we have seen that, for a naturalness [32] favored region of

SUSY spectra with a given $\tan\beta$, the ratio of neutralino to chargino contributions within a_μ^{SUSY} in minimal AMSB is typically smaller by 50% or so, compared to the same within a similar natural mSUGRA spectra.

4.1 Constraints from present values of a_μ^{exp} and a_μ^{SM}

Figs. (3a) to (3d) show the constraints arising from a_μ^{SUSY} , from the present experimental data from Brookhaven and the Standard model result. Here we consider the residual amount $a_\mu^{\text{expt}} - a_\mu^{\text{SM}}$ to limit a_μ^{SUSY} within 2σ level of combined error estimates, added in quadratures ($-45.7 \times 10^{-10} < a_\mu^{\text{SUSY}} < 140.1 \times 10^{-10}$). Considering the largest possible $|a_\mu^{\text{SUSY}}|$ within the model, we see that, essentially a constraint exists only for $\mu < 0$. The regions excluded by a_μ^{SUSY} bounds when combined with the disallowed regions (labeled by X) characteristic in the minimal AMSB model itself, along with the experimental constraints on various sparticle masses, a value of m_0 below 275 GeV is completely eliminated for any value of $m_{3/2}$ (see Fig. (3a)). The same for $\tan\beta = 40$ as shown in Fig. (3c) amounts to $m_0 \sim 375$ GeV. Additionally, as seen in the same displays, significantly larger m_0 values than what are mentioned above, are excluded for a limited region of $m_{3/2}$.

Constraining minimal AMSB model via a_μ^{SUSY} can be further effective in the $(m_{\tilde{\chi}_1^\pm}, m_{\tilde{\nu}_\mu})$ plane (see Figs.(3b) and (3d)) because as noted earlier, the chirality non-diagonal lighter chargino terms dominate over the other contributions. A value of $m_{\tilde{\nu}_\mu}$ below 225 (325) GeV for $\tan\beta = 25(40)$ is explicitly ruled out via the current limit on a_μ^{SUSY} . Here we note that, in situations similar to the minimal AMSB model, where $m_{\tilde{\chi}_1^\pm}$ and $m_{\tilde{\chi}_1^0}$ masses are almost degenerate, and sneutrinos are light, the present experimental lower bound of $m_{\tilde{\chi}_1^\pm}$ is 56 GeV[33]. The white regions denoted by X in the bottom of the a_μ^{SUSY} -allowed and disallowed zones of Figs.(3b) and (3d) are disallowed by the model itself, and we will further comment on them while discussing similar regions of Figs.(4) and (5).

4.2 Probing minimal AMSB scenario further, via a_μ^{SUSY} and BNL experiment at its predicted level of accuracy

The uncertainty level of $\delta a_\mu^{\text{BNL}} = 4 \times 10^{-10}$, which is going to be achieved in Brookhaven within a few years, will at least, significantly constrain the parameter space of a Beyond

the Standard Model theory. Considering this predicted level of accuracy, we constrain a_μ^{SUSY} within 2σ limit (see Figs.(4) and (5)), where σ is obtained from the predicted uncertainty level of BNL measurement and the error associated with SM result, added in quadratures. The assumed non-differing central estimates of experimental and theoretical results, would be the limiting scenario of seeing no deviation from the Standard Model result. This analysis would be valid in the situation, when the experiment is complete, and no deviation from the Standard Model is seen within error limits. This is in similar line to what have been seen in Refs.[5, 34] for supersymmetric as well as non-supersymmetric theories. On a further note, we assume that, the hadronic error in a_μ^{had1} would be staying at its present level. A reduction on the other hand, which will occur in the near future, would further constrain a similar analysis.

The lower triangular regions in $(m_{3/2}, m_0)$ plane of Figs. (4) and (5) are the disallowed zones, where $|a_\mu^{\text{SUSY}}|$ exceeds the 2σ limit of the combined uncertainty. The same result within the a_μ^{SUSY} -relevant mass pairs $(m_{\tilde{\chi}_1^\pm}, m_{\tilde{\nu}_\mu})$ is presented in the right hand sides of Figs.(4) and (5). We note that, corresponding to $\tan\beta=10$ and 25, the minimal AMSB satisfied parameter space is reasonably identical, with respect to the sign of μ . In Figs.(4e) and (5e) however, the regions differ in this aspect, and we will come back to them in Section 5.

Fig.(4) and (5) indicate that $m_0 < 275$ (475) GeV domains will be entirely eliminated for $\tan\beta = 10$ (25) for both signs of μ . For $\tan\beta = 40$, the corresponding limits are 625 GeV for $\mu < 0$ and 800 GeV for $\mu > 0$. The limit of $m_0 \leq 800$ GeV for $\mu > 0$ appears out of reasons which we will discuss soon. Within $(m_{\tilde{\chi}_1^\pm}, m_{\tilde{\nu}_\mu})$ planes of the right hand side of Fig.(4) and (5), we find that for $\mu < 0$ and $\tan\beta = 10, 25$ and 40, values of $m_{\tilde{\nu}_\mu}$ less than 210, 400 and 560 GeV are excluded. The situation for $\mu > 0$ is identical for $\tan\beta = 10$ and 25. A significant difference between the signs of μ can be seen now, switching to $\mu > 0$ and $\tan\beta = 40$. Similar disallowed range will be very stringent here, namely $m_{\tilde{\nu}_\mu}$ below 780 GeV will be excluded.

Interestingly, an important result is found, when this analysis of a_μ^{SUSY} is combined with $b \rightarrow s + \gamma$ constraint. The constraint from $b \rightarrow s + \gamma$ within minimal AMSB scenario as analyzed in Ref. [13], is somewhat complementary to what we find here from a_μ^{SUSY} . This is because, $b \rightarrow s + \gamma$ calculation, which has many special features in AMSB models, puts severe mass limits for $\mu > 0$, and much smaller limits for $\mu < 0$. On the other hand,

within the above scenario of seeing no deviation from SM result once the experiment is performed at the predicted level of accuracy, a_μ^{SUSY} limit in the minimal AMSB model, shows a very significant constraint for both $\mu < 0$ and $\mu > 0$ cases.

5 Generally disallowed parameter zones

A discussion about the generally eliminated parameter space may be useful in studying the supersymmetric contribution to muon $(g - 2)$ in a given SUSY model, because a combined constraint from a_μ^{SUSY} , as well as from any generic disallowedness results in simpler and definite predictions. Restricting stau from turning tachyonic corresponds to a significant constraint in AMSB models. In this section, by *allowedness* we would mean valid input parameters from the model along with various experimental lower bounds of sparticle masses, without reference to any a_μ^{SUSY} constraint.

We will first describe few observations as revealed from our numerical analysis. For a given m_0 , the larger $m_{3/2}$ values falling within the region labeled by X , in Figs. (4) and (5) are eliminated because of decreasing stau mass ($m_{\tilde{\tau}_1}$), which either goes below the experimental lower limit of 70 GeV[35], or it becomes the LSP, hence discarded in our R-parity conserved scenario. Thereafter, with further increase of $m_{3/2}$, stau turns tachyonic. We also see that the maximum possible $m_{3/2}$ for a given m_0 , as allowed by the minimal AMSB model, is larger for a smaller $\tan\beta$. Thus, for $\mu < 0$ and $m_0 = 400$ GeV, comparing Fig. (4a), Fig. (4c), and Fig. (4e) we find that such maximum possible values of $m_{3/2}$ are approximately 67, 52 and 41 TeV for $\tan\beta = 10, 25$ and 40 respectively. On the other hand, for a given $\tan\beta$, allowed $m_{3/2}$ increases for an increase in m_0 . Besides, smaller $m_{3/2}$ regions below the origins of the displays, are eliminated via the experimental constraint of $m_{\tilde{\chi}_1^\pm} \gtrsim 56\text{GeV}$ [33].

We will try to explain qualitatively, the behavior of stau mass with variations of the basic parameters of the model. The effect of $\tilde{\tau}_1$ becoming tachyonic as described above, is best explained via \tilde{m}_L^2 (see Eq. (5) for $i \equiv L$) assuming smaller left-right slepton mixing for convenience. There are two effects in \tilde{m}_L^2 due to a change in $\tan\beta$, which may support or oppose each other. The first one arises from the scale invariant part of \tilde{m}_L^2 and, the other one originates from the RG evolution[28] of the same.

The Yukawa term in the scale invariant part of \tilde{m}_L^2 in Eq. (5) is intrinsically negative,

itself being also gauge coupling dominated within the corresponding $\hat{\beta}$ function, for the range $\tan\beta$ considered in this analysis. Hence, the value of \tilde{m}_L^2 at M_G decreases if $\tan\beta$ is larger. We consider here moderate values of m_0 for simpler discussion. Until $\tan\beta$ is in a smaller domain, so that τ -Yukawa coupling (h_τ) within the scalar mass RG equation[28] may be neglected compared to the gauge terms, the RGE effect due to running from M_G to the electroweak scale always increases \tilde{m}_L^2 , because of gauge domination. Thus the two effects oppose each other. But, within smaller $\tan\beta$ domains, regarding the value of \tilde{m}_L^2 at the electroweak scale for an increase in $\tan\beta$, the effect of AMSB specified decrease in \tilde{m}_L^2 at M_G is stronger than the increase due to the RGE effect. This we have also verified numerically in a broad domain of parameter ranges. As a result, \tilde{m}_L^2 and consequently $m_{\tilde{\tau}_1}$ decreases with increase in $\tan\beta$. This in turn means that, for a given m_0 , the upper limit of $m_{3/2}$ is reached sooner for a larger $\tan\beta$. This we may see from Figs. (4) and (5), as well as from the values quoted above within this section.

For a further increase in $\tan\beta$ (~ 40 in our analysis), instead of opposing, the two effects may go in the same direction, although with varying strengths, because the τ -Yukawa term may now start to dominate within the RG evolution. In fact, this may also be true when m_0 is large, with $\tan\beta$ in a moderately larger domain (~ 25).

On the other hand, corresponding to the lowest $m_{3/2}$ values satisfying the lighter chargino experimental bound, a gradual increase of lower limit of m_0 with increase in $\tan\beta$ is found (see left side displays of Fig.(4) and (5)), because as explained before, the scale invariant part of \tilde{m}_L^2 turns further negative for increasing $\tan\beta$, and larger m_0 values are hence needed to compensate. However, there is a marked difference between $\mu < 0$ and $\mu > 0$ cases, for $\tan\beta = 40$ (see Fig.(4e) and (5e)). The upper limit of the $m_{3/2}$ for $\mu > 0$ as allowed by the model, is much smaller compared to the same for $\mu < 0$. This happens due to a generic large $\tan\beta$ effect, the effect of large SUSY-QCD loop corrections of bottom quark mass[30]. Significantly, this correction has special features in AMSB scenario [18], because within the same, the $SU(3)$ gaugino mass \tilde{m}_3 comes with a negative sign. Consequently, for $\mu > 0$ and large $\tan\beta$, due to a large SUSY QCD loop correction, a very large h_b ($\sim h_t$) causes $m_{H_d}^2$ for Higgs scalar to turn sufficiently negative so that the CP-odd Higgs particle becomes tachyonic. However, here $\tilde{\tau}_1$ can still remain non-tachyonic. A further increase of $m_{3/2}$ affects $\tilde{\tau}_1$ to become tachyonic, as usual.

Considering now the combined effect of the model specified disallowed space, as well

as the constraint from a_μ^{SUSY} , we can see that a region below $m_0 = 800$ for $\mu > 0$ will be completely eliminated within the scenario of seeing no deviation from SM. The right hand side displays of the Figs.(4) and (5) also show model-specified eliminated regions, as identified by X in $(m_{\tilde{\chi}_1^\pm}, m_{\tilde{\nu}_\mu})$ plane. Obviously, the masses are not independent, because they are derived from the basic set of input-parameters of the minimal AMSB model. The same reason of $\tilde{\tau}_1$ turning tachyonic eliminates a large region within the zones X . The disallowed X -zone is large for $\mu > 0$ and $\tan\beta = 40$ in Fig.(5f), compared to the same for $\mu < 0$, as shown in Fig.(4f). This occurs because of the same reason for which the upper limit of $m_{3/2}$ is smaller in Fig.(5e) which we have explained before, and due to the fact that the lighter chargino is wino dominated within AMSB, thus $m_{\tilde{\chi}_1^\pm}$ being almost proportional to $m_{3/2}$.

6 Conclusion

We have computed the supersymmetric contribution to anomalous magnetic moment of muon within minimal Anomaly Mediated Supersymmetry Breaking model. There are one-loop contributions involving chargino-sneutrino, and neutralino-smuon parts. The chiral interference term involving lighter chargino is seen to contribute the most to a_μ^{SUSY} , than the other chargino and neutralino terms, and this also results in a definite sign relationship between a_μ^{SUSY} and μ . Besides, this also gives an almost proportional relationship of $|a_\mu^{\text{SUSY}}|$ with $\tan\beta$. We have also seen the effect of large smuon L-R mixing which causes strong partial cancellations between the various terms of neutralino result of a_μ^{SUSY} . This is a significantly important result of a_μ^{SUSY} within minimal AMSB.

We have analyzed the constraint coming from current values of a_μ from the Standard Model and the ongoing experiment at Brookhaven, assuming that the difference appears due to SUSY. The constraint which exists only for $\mu < 0$ shows that, for $\tan\beta = 25$ (40), regions with $m_0 < 275$ (375) GeV, and correspondingly $m_{\tilde{\nu}_\mu} < 225$ (325) GeV are eliminated. We have also investigated the constraint from a_μ^{SUSY} that would result, if the Brookhaven experiment with its already predicted level of accuracy finds no deviation from the Standard Model result. In this scenario, one finds that for $\mu < 0$ and $\tan\beta = 10, 25$ and 40, the lower bounds of m_0 would be 275, 475 and 625 GeV, while the corresponding lower limits for $m_{\tilde{\nu}_\mu}$ would be 210, 400 and 560 GeV respectively. The lower bounds for $\mu > 0$

are identical with $\mu < 0$, except for $\tan\beta = 40$, where $m_0 < 800$ and correspondingly $m_{\tilde{\nu}_\mu} < 780$ GeV regions would be excluded. This happens due to a large SUSY-QCD correction to the bottom quark mass, a large $\tan\beta$ effect.

We have also compared our constraint with the same obtained from $b \rightarrow s + \gamma$ from Ref. [13]. We found that the high accuracy level of the BNL experiment will be very useful to constrain the model for $\mu < 0$, because $b \rightarrow s + \gamma$ limit is effective only for $\mu > 0$. Furthermore, we have also analyzed the generically disallowed zones within the parameter space of the model, because a combined constraint from a_μ^{SUSY} and such invalid parameter ranges leads to a stronger prediction.

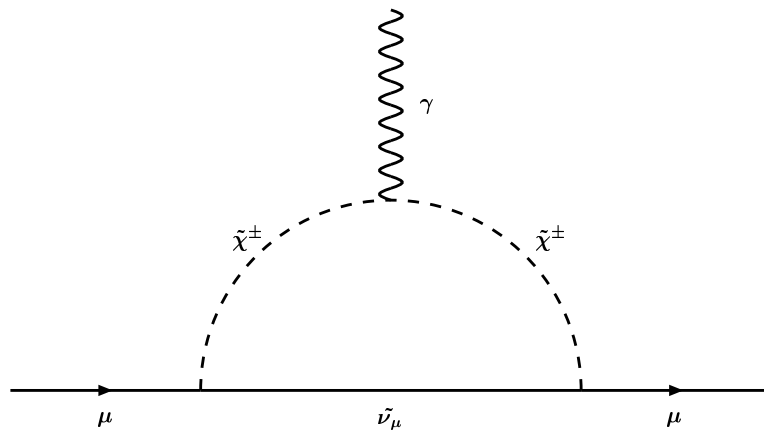
Acknowledgment: DKG wishes to acknowledge the hospitality provided by the Theory Division, CERN, where part of this work was completed.

References

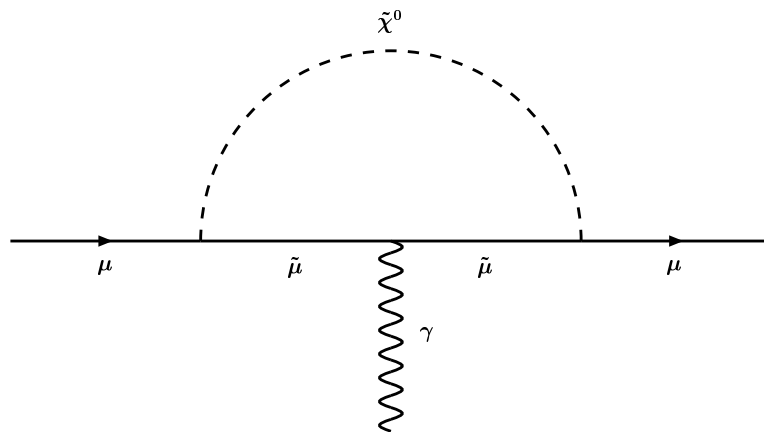
- [1] B. L. Roberts, *Status of the Muon ($g-2$) Experiment*, XIX International Symposium on Lepton and Photon Interactions at High Energy, Stanford University, August 1999, hep-ex/0002005; R. M. Carey *et al.*, Phys. Rev. Lett. **82**, 1632 (1999); D. Hertzog *et al.* *The New Brookhaven ($g_\mu - 2$) Experiment*, Sixth International Symposium on Particles, Strings and Cosmology (PASCOS 98), Northeastern University, Boston, March 1998, World Scientific;
URL: <http://www.g2muon.bnl.gov> & <http://www.phy.bnl.gov/g2muon/home.html>.
- [2] J. Bailey *et al.*, Phys. Lett. **68B**, 191 (1977); Nucl. Phys. **B150**, 1 (1979).
- [3] T. Ibrahim and P. Nath, hep-ph/9908443.
- [4] G. Cho, K. Hagiwara and M. Hayakawa, Phys.Lett. **B478**, 231 (2000); T. Blažek, hep-ph/9912460; T. Moroi, Phys. Rev. **D53**, 6565 (1996); Erratum-*ibid.* **D56** 4424 (1997); M. Carena, G.F. Giudice and C.E.M. Wagner, Phys. Lett. **B390**, 234 (1997).
- [5] U. Chattopadhyay and P. Nath, Phys. Rev. **D53**, 1648 (1996).
- [6] T. Goto, Y. Okada and Y. Shimizu, hep-ph/9908499; T. Ibrahim and P. Nath, Phys.Rev. **D61**, 095008,(2000); J.L. Lopez, D.V. Nanopoulos and X. Wang, Phys. Rev. **D49**, 366 (1994) and references therein; T.C. Yuan, R. Arnowitt, A.H. Chamseddine, and P. Nath, Z. Phys. **C26**, 407 (1984).
- [7] K. T. Mahanthappa and S. Oh, *Proceedings of the International Europhysics Conference on High Energy Physics*, Tampere, Finland, July, 1999 (hep-ph/9909410); Carena *et al.* of Ref. [4].
- [8] P. Nath, R. Arnowitt and A.H. Chamseddine, Applied N=1 Supergravity, ICTP Lecture Series, Vol-I, 1983 (World Scientific, Singapore 1984); H. P. Nilles, Phys. Rep. **110**, 1 (1984).
- [9] G.F. Giudice and R. Rattazzi, Phys. Rept. **322**, 419-499 (1999); *ibid.* Phys. Rept. **322**, 501 (1999).
- [10] L. Randall and R. Sundrum, Nucl. Phys. **B557**, 79 (1999).

- [11] G.F. Giudice, M.A. Luty, H. Murayama, and R. Rattazzi, JHEP **9812**, 027 (1998).
- [12] J.A. Bagger, T. Moroi, and E. Poppitz, JHEP **0004**, 009 (2000).
- [13] J.L. Feng and T. Moroi, Phys. Rev. D **61**, 095004 (2000).
- [14] T. Gherghetta, G.F. Giudice, and J.D. Wells, Nucl. Phys. **B559**, 27 (1999).
- [15] S. Su, Nucl.Phys. **B573**, 87 (2000).
- [16] J.L. Feng, T. Moroi, L. Randall, M. Strassler, and S. Su, Phys. Rev. Lett. **83**, 1731 (1999); F. Paige and J. Wells, hep-ph/0001249.
- [17] D.K. Ghosh, P. Roy, and S. Roy, hep-ph/0004127.
For other interesting collider aspects within minimal AMSB see Ref. [14, 16].
- [18] G.D. Kribs, Phys. Rev. **D62**, 015008 (2000).
- [19] A. Czarnecki and W. J. Marciano, Invited talk at the 5th International Workshop on Tau Lepton Physics (Tau'98), September 1998, Santander, Spain, hep-ph/9810512; T. Kinoshita, Phys. Rev. **D47**, 5013 (1993).
- [20] M. Davier and A. Höcker, Phys. Lett. **B435**, 427 (1998).
- [21] B. Krause, Phys. Lett. **B 390**, 392 (1997).
- [22] M. Hayakawa, T. Kinoshita and A.I. Sanda, Phys. Rev. Lett. **75**, 790 (1995); *ibid.* Phys. Rev. **D54**, 3137 (1996).
- [23] T. Kinoshita and W.J. Marciano, in *Quantum Electrodynamics*, ed. T. Kinoshita (World Scientific, Singapore, 1990), pp. 419-478; T. Kinoshita, B. Nizic, and Y. Okamoto, Phys. Rev. **D31**, 2108 (1985); T. Kinoshita, Z. Phys. **C56**, S80 (1992).
- [24] *BEPC and the Future Program at IHEP*, Z.T. Zhao, S.H. Wang, First Asian Particle Accelerator Conference (APAC 98), Tsukuba, Japan, 23-27 Mar 1998;
Physics at DAPHNE, G. Pancheri, Acta Phys. Polon. **B30**, 2243 (1999);
Status of Experiments and Recent Results from CMD-2 Detector at VEPP-2M, Third Workshop on Physics and Detectors for DAPHNE (DAPHNE 99), Frascati, Italy, 16-19 Nov 1999, hep-ex/0001049.

- [25] F. Jegerlehner, *IVth International Symposium on Radiative Corrections, Barcelona, September 1998* (hep-ph/9901386).
- [26] A. Pomarol and R. Rattazzi, JHEP **9905**, 013 (1999); E. Katz, Y. Shadmi and Y. Shirman, JHEP **9908**, 015, (1999); Z. Chacko, M.A. Luty, I. Maksymyk, and E. Ponton, JHEP **0004**, 001 (2000); I. Jack and D. R. T. Jones, hep-ph/0003081; B.C. Allanach and A. Dedes, hep-ph/0003222; M. Carena, K. Huitu, and T. Kobayashi, hep-ph/0003187; R. Rattazzi, A. Strumia, J.D. Wells, hep-ph/9912390.
- [27] J.L. Feng, K. Matchev and T. Moroi, Phys. Rev. **D61**, 075005 (2000).
- [28] S.P. Martin and M.T. Vaughn, Phys. Rev. **D50**, 2282 (1994).
- [29] R. Arnowitt and P. Nath, Phys. Rev. **D46**, 3981 (1992); V. Barger, M.S. Berger and P. Ohmann, Phys. Rev. **D49**, 4908 (1994).
- [30] L.J. Hall, R. Rattazzi and U. Sarid, Phys. Rev. **D50**, 7048 (1994); R. Hempfling, Phys. Rev. **D49**, 6168 (1994); M. Carena, M. Olechowski, S. Pokorski and C. Wagner, Nucl. Phys. **B426**, 269 (1994); D. Pierce, J. Bagger, K. Matchev and R. Zhang, Nucl. Phys. **B491**, 3 (1997).
- [31] H. Baer, M. Díaz, P. Quintana and X. Tata, JHEP **0004**, 016 (2000).
- [32] For naturalness in mSUGRA, see Ref. [27] and K.L. Chan, U. Chattopadhyay and P. Nath, Phys. Rev. **D58**, 096004 (1998) and references therein;
For naturalness within minimal AMSB, see Ref. [13].
- [33] M. Maltoni, hep-ph/0003315.
- [34] T. Blažek of Ref. [4]; For an analysis in two Higgs doublet model see: M. Krawczyk and J. Zochowski, Phys.Rev. **D55**, 6968 (1997).
- [35] LEP SUSY Working Group, ALEPH, DELPHI, L3, OPAL experiments, note LEPSUSYWG/99-01.1.



(a)



(b)

Figure 1: Feynman diagrams contributing to a_μ^{SUSY} ; (a) for chargino-sneutrino loop, (b) for neutralino-smuon loop.

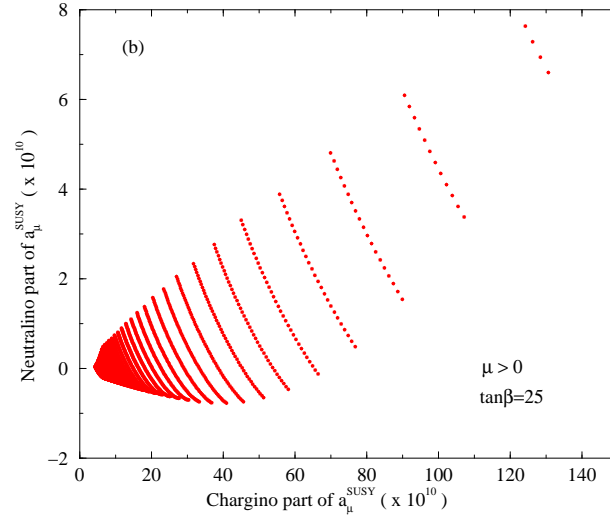
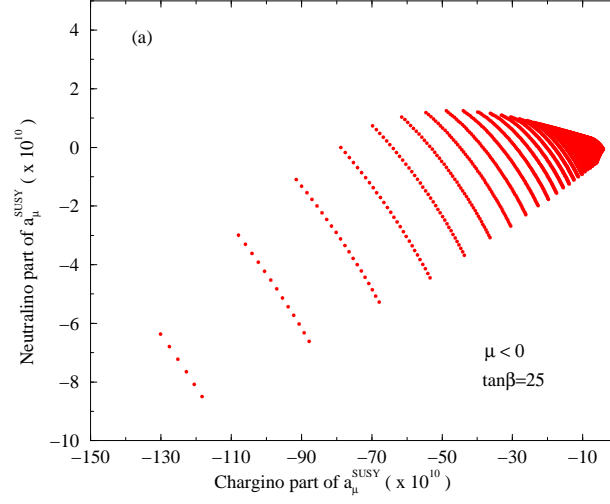


Figure 2: Relative contributions to muon a_μ^{SUSY} for (a) $\mu < 0$ and (b) $\mu > 0$ from chargino-sneutrino and neutralino-smuon loops when $\tan\beta = 25$, and $m_0 \leq 1000$ GeV and $m_{3/2} \leq 100$ TeV.

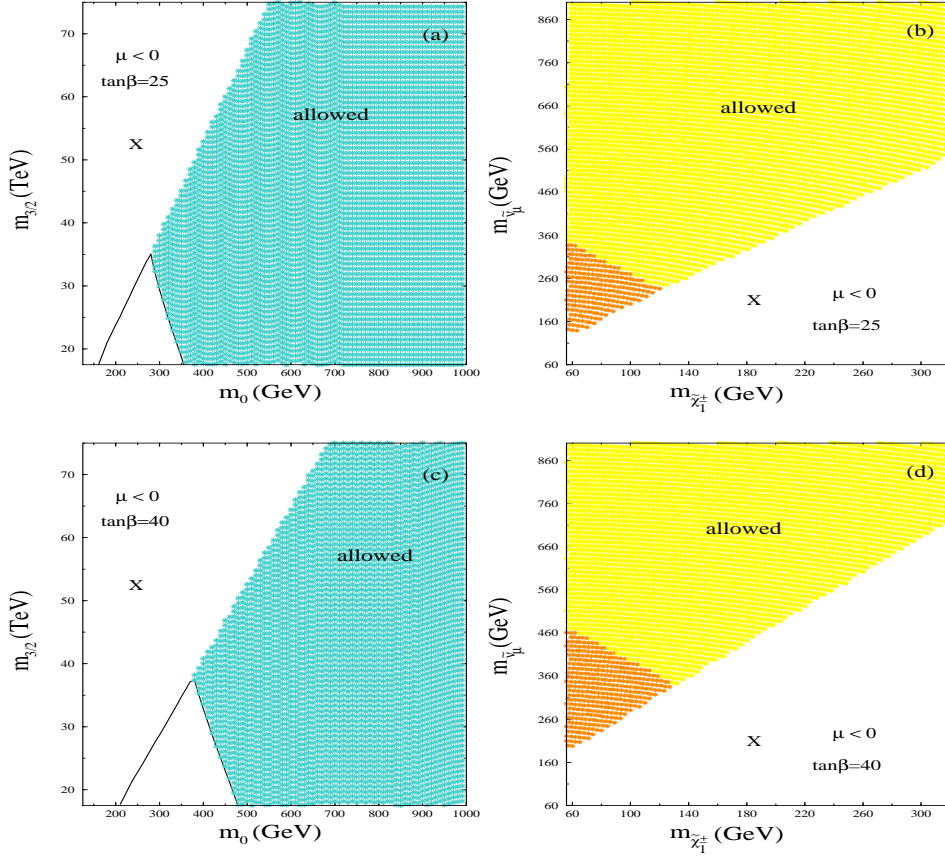


Figure 3: Constraints in $(m_0 - m_{3/2})$ and $(m_{\tilde{\chi}_1^\pm} - m_{\tilde{\nu}_\mu})$ plane from present limits of a_μ^{SUSY} for $\mu < 0$. Regions allowed by a_μ^{SUSY} constraint are labeled as *allowed*. Regions marked with *X* are generally disallowed zones for the SUSY spectra within minimal AMSB. Small white triangular regions below the *allowed* areas in the left hand side figures are disallowed via a_μ^{SUSY} limit. Same regions in the right hand side are darkly shaded.

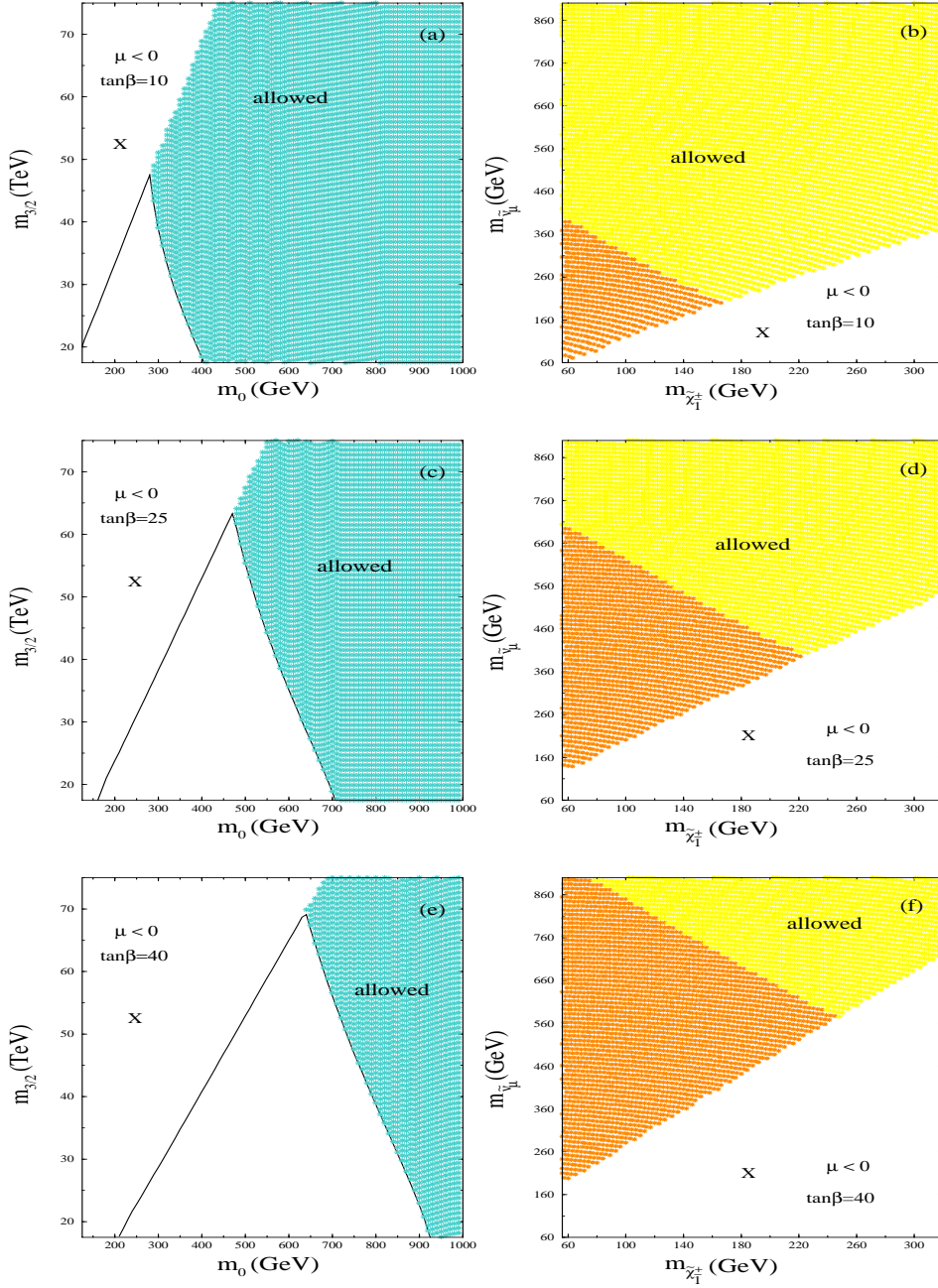


Figure 4: Constraints in $(m_0 - m_{3/2})$ and $(m_{\tilde{\chi}_1^\pm} - m_{\tilde{\nu}_\mu})$ plane within *no deviation from SM* scenario of a_μ^{SUSY} as explained in the text for $\mu < 0$. Regions allowed by a_μ^{SUSY} constraint are labeled as *allowed*. Regions marked with *X* are generally disallowed zones for the SUSY spectra within minimal AMSB. White triangular regions below the *allowed* areas in the left hand side figures are disallowed via a_μ^{SUSY} limit. Same regions in the right hand side are darkly shaded.

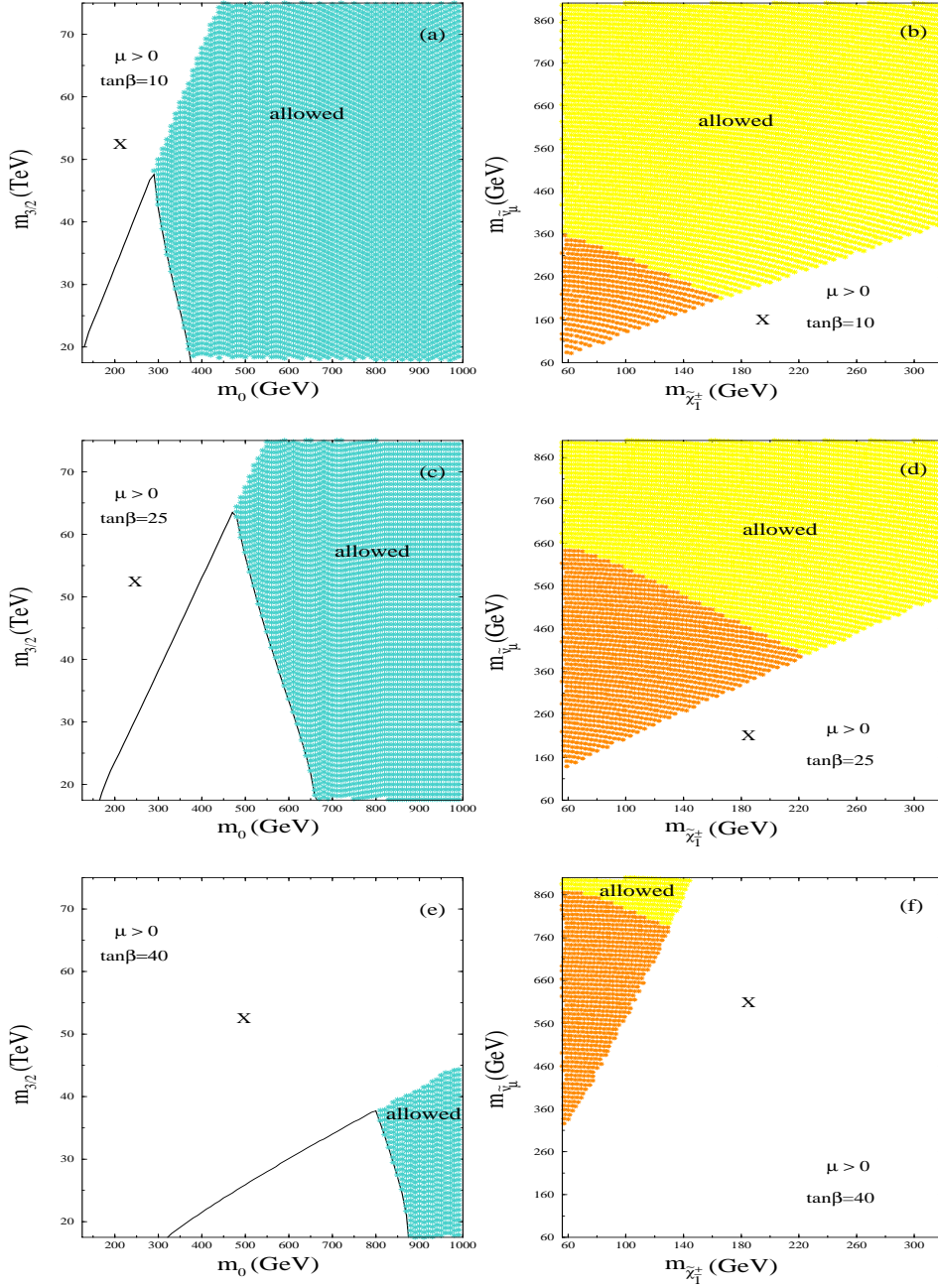


Figure 5: Constraints in $(m_0 - m_{3/2})$ and $(m_{\tilde{\chi}_1^\pm} - m_{\tilde{\nu}_\mu})$ plane within *no deviation from SM* scenario of a_μ^{SUSY} , as explained in the text for $\mu > 0$. Regions allowed by a_μ^{SUSY} constraint are labeled as *allowed*. Regions marked with *X* are generally disallowed zones for the SUSY spectra within minimal AMSB. White triangular regions below the *allowed* areas in the left hand side figures are disallowed via a_μ^{SUSY} limit. Same regions in the right hand side are darkly shaded.